

Shape from Fluorescence

Tali Treibitz¹, Zak Murez¹, B. Greg Mitchell², and David Kriegman¹

¹ Department of Computer Science and Engineering

² Scripps Institution of Oceanography,

University of California, San Diego

{tali,zmurez,gmitchell,kriegman}@ucsd.edu

Abstract. Beyond day glow highlighters and psychedelic black light posters, it has been estimated that fluorescence is a property exhibited by 20% of objects. When a fluorescent material is illuminated with a short wavelength light, it re-emits light at a longer wavelength isotropically in a similar manner as a Lambertian surface reflects light. This hitherto neglected property opens the doors to using fluorescence to reconstruct 3D shape with some of the same techniques as for Lambertian surfaces – even when the surface’s reflectance is highly non-Lambertian. Thus, performing reconstruction using fluorescence has advantages over purely Lambertian surfaces. Single image shape-from-shading and calibrated Lambertian photometric stereo can be applied to fluorescence images to reveal 3D shape. When performing uncalibrated photometric stereo, both fluorescence and reflectance can be used to recover Euclidean shape and resolve the generalized bas relief ambiguity. Finally for objects that fluoresce in wavelengths distinct from their reflectance (such as plants and vegetables), reconstructions do not suffer from problems due to inter-reflections. We validate these claims through experiments.

Keywords: 3D Reconstruction, Photometric Stereo, Shape from Shading, Fluorescence, Subsurface Scattering.

1 Introduction

When a material fluoresces, it absorbs light at a shorter wavelength and emits it at a longer wavelength. For example, when illuminated by blue light, Chlorophyll fluoresces red (Fig. 1). Minerals emit a wide variety of visible colors when illuminated by ultraviolet (UV) light. While it has been reported that 20% of materials fluoresce [1], most models of color and reflectance in computer vision neglect fluorescence.

Radiometric methods for reconstructing shape such as single image shape-from-shading, photometric stereo, and passive photometric stereo from motion develop explicit models relating illumination, surface reflectance, and image irradiance. Central to these methods is the bidirectional reflectance distribution function (BRDF) which can be considered as being wavelength dependent. For example, in classic photometric stereo of surfaces with arbitrary reflectance,

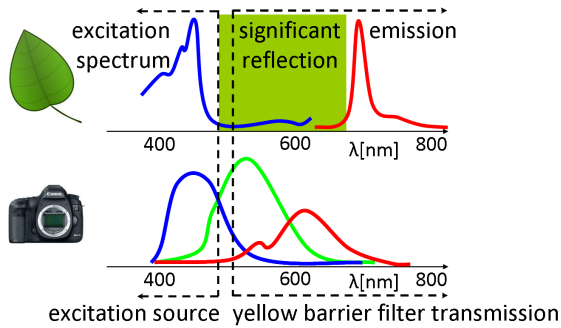


Fig. 1. [Top] Chlorophyll-a excitation and emission spectra. The excitation peak is at 430nm and the emission peak is at 685nm. Wavelengths at the green range are not absorbed and thus reflected, giving the plants their prominent green color. [Bottom] Spectral sensitivities of the RGB channels in a Canon 5DII camera. The excitation spectrum has almost no overlap with the red camera channel. The yellow barrier filter over the lens enables imaging of green fluorescence (such as Green Fluorescent Proteins) without contamination of the excitation light. Although theoretically it seems that the yellow filter is not necessary for red fluorescence imaging, in practice, the excitation intensity is much stronger than the emission intensity, and so any leakage of longer wavelength of light from the blue source would reflect and appear in the red channel. The barrier filter reduces leakage and leads to correct exposure of the red channel.

reflectance maps are either derived from the BRDF for each light source direction [2] or measured from a reference object of the same material [3]. Under Lambertian reflectance, the measured image irradiance is independent of the viewing direction. Then, surface normals are readily estimated from three or more images as the solution of a linear system of equations [2], and a spatially varying albedo can also be estimated. In addition, many computer vision algorithms that rely on the constant brightness assumption (e.g., optical flow, dense stereo matching, space carving) implicitly or explicitly assume that surfaces are Lambertian. Unfortunately few materials are truly Lambertian except manufactured materials like Spectralon, and so one must often contend with non-Lambertian surfaces and this significantly complicates reconstruction compared to the simplicity and robustness of methods for Lambertian surfaces.

Until now, fluorescent materials were mainly used in computer vision and graphics to enhance visibility and contrast when imaging in scattering media [4]. The property that the fluorescence color is distinct from the illumination color is used to optically filter out at the camera the wavelengths corresponding to the illuminant while allowing the wavelengths of the fluorescence emission from the object to pass. Fluorescence was also used to reconstruct transparent objects. Ihrke et al. [5] added a fluorescent dye to water to enable reconstruction of flow from a video sequence. Hullin et al. [6] immerse transparent objects in a fluorescent solution to enable range scanning techniques.

Interestingly, fluorescent emissions are almost always isotropic [7], radiating energy equally in all directions, albeit at a different wavelength than the incident illumination. Consequently, it has the same behavior as an ideal Lambertian

surface. In this paper, we exploit this phenomenon to estimate shape from fluorescence in images. Contemporary with this paper, Sato et al. [8] presented similar contributions.

2 Image Formation

2.1 Reflectance

For simplicity of development, we consider an object surface point to be illuminated by a single light source from the incident direction in polar coordinates (θ_i, ϕ_i) with an incident radiance $L_i(\lambda)$. The object is viewed by a camera from the direction (θ_r, ϕ_r) , also in polar coordinates. The amount of light reflected from the object point towards the camera [9] is expressed by

$$L_r(\lambda) = L_i(\lambda)F(\lambda, \boldsymbol{\theta}) \cos \theta_i \quad , \quad (1)$$

where $F(\lambda, \boldsymbol{\theta})$, is the BRDF at this object point, and $\boldsymbol{\theta} = (\theta_i, \phi_i, \theta_r, \phi_r)$, are incident and viewing directions in spherical angles relative to a local coordinate system defined by the surface normal. The $\cos \theta_i$ term is a foreshortening factor, as the exposed surface area decreases as the angle between the surface normal and illumination direction increases.

The intensity of a pixel in color channel c with sensitivity $z_c(\lambda)$ is

$$I_c = k(\gamma) \cos \theta_i \int_A z_c(\lambda) L_i(\lambda) F(\lambda, \boldsymbol{\theta}) d\lambda \quad , \quad (2)$$

where A is the range of visible wavelengths. Here k is the ratio between image irradiance and scene radiance [10], which depends on the effective f-number, lens transfer function, etc. In addition, k depends on γ , the angle between the projected ray to the optical axis [10]. Most algorithms reconstructing shape from illumination assume the camera is viewing all object points from the same direction (orthographic projection), so that $k(\gamma)$ becomes a constant, or estimate $k(\gamma)$ through calibration. Either way, from here on we assume the dependency on γ was corrected and treat k as a constant.

Typical BRDFs can be divided into two types of reflections. A *specular reflection* is mirror-like where most of the incident light at the surface is reflected and concentrated about the reflection angle $\theta_r = \theta_i$. On the other hand, a *diffuse* surface reflects light towards a wide range of angles. An ideal *Lambertian* surface reflects light uniformly towards all directions, and the BRDF is equal to the surface albedo

$$F(\lambda, \boldsymbol{\theta}) = F(\lambda) \quad . \quad (3)$$

Plugging Eqs. (1,3) into Eq. (2) yields the image intensity for a Lambertian surface

$$I_c = a_c \mathbf{L} \cdot \mathbf{N} \quad , \quad (4)$$



Fig. 2. Common fluorescent objects. In each example, the color image on the left was acquired under white light whereas the image on the right was acquired under blue light with a yellow filter over the lens. (a) Plastic objects (as well as papers) often fluoresce under a wide excitation spectrum. They are made fluorescent at the same color they reflect to appear especially bright. The color of the “ice cream” on the right is due to fluorescence; since the cone does not fluoresce and only reflects, it appears black in the fluorescence image. (b) Green plants and vegetables contain Chlorophyll that fluoresces red. The image on the right was taken with a camera with a removed IR filter, for increased sensitivity for Chlorophyll fluorescence [15].

where \mathbf{L} is a illumination direction scaled by the light source strength and \mathbf{N} is the unit surface normal. The term a_c is the sensed color of the object in the channel c , as a function of the albedo, light spectrum and the channel sensitivity

$$a_c = k(\gamma) \int_{\Lambda} z_c(\lambda) L_i(\lambda) F(\lambda) d\lambda . \quad (5)$$

Ideal Lambertian reflectance hardly exists in nature. Thus, there is a wide literature on models of non-Lambertian reflectance that aim to characterize either very specific material classes with a few parameters or a wide range of materials with many parameters. Some of the prominent ones are Oren-Nayar [11], Phong [12], Cook-Torrance [13] and Ashikmin-Shirley [14].

2.2 Fluorescence

Stokes fluorescence, the common observed type of fluorescence, is the re-emission of photons having longer wavelengths than the absorbed photons [4]. Any fluorescent molecule has two characteristic spectra. The excitation spectrum is the relative efficiency of different wavelengths of the exciting radiation to cause fluorescence. The emission spectrum is the relative intensity of radiation emitted at various wavelengths (example in Fig. 1). To image just the fluorescence, an excitation filter is mounted on a light source, or a narrow band light source such as a laser or LED is used. In addition, an emission filter is mounted on the camera. These filters are designed to have sharp boundaries, and to have negligible overlap in their transmittance spectra. Recently, Zhang and Sato [16] proposed a method for separating reflectance and fluorescence by using two images illuminated by distinct colored light sources, that can have some overlap. In microscopy, narrow band filters are used to image various fluorescent molecules, that are later unmixed [17] to yield the separate emitted fluorescence signals.

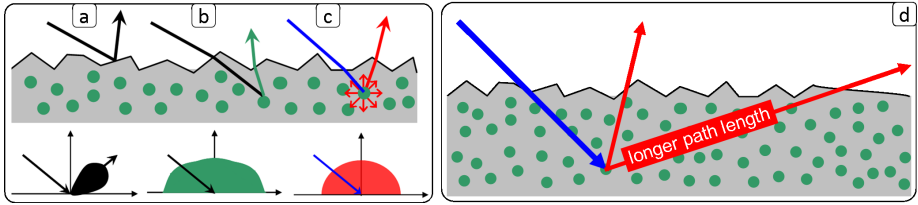


Fig. 3. Scattering effects in a fluorescent object: (a) Specular reflections from the surface are concentrated in a specular lobe around the specular angle $\theta_r = \theta_i$ and often resemble the illumination color; (b) Light that penetrates the surface undergoes scattering and eventually part of it is reflected back to the viewer taking on the body color. The shape of the diffuse BRDF, which includes ideal Lambertian reflectance, varies among surfaces and depends on the surface roughness [11], among other factors; (c) Fluorescence emission of particles is often isotropic, and thus the surface emission is close to be ideally Lambertian; (d) Differences in optical path length from the fluorescence emission to the surface might harm isotropy due to absorption.

Fluorescence is more abundant in everyday life than is usually acknowledged, and examples of fluorescent objects are shown¹ in Fig. 2. Many papers and plastics are made fluorescent to have a more striking color. Bleaching detergent is fluorescent and as a result, white papers and many cloths fluoresce as well. In nature, green fruits, vegetables and plants fluoresce due to Chlorophyll. This photosynthetic pigment strongly absorbs blue and red irradiance and reflects green. Part of the blue irradiance is converted to fluorescence in the red spectrum. Excitation and emission spectra of Chlorophyll are shown in Fig. 1. Corals fluoresce in red and green as they contain both Chlorophyll and Green Fluorescent Proteins. While less significant in every day life because of atmospheric attenuation, many objects fluoresce when excited by UV light. Many minerals fluoresce under UV in colors of red, orange, yellow, green, blue, violet, etc. Porphyrins in the human skin fluoresce under UV and are used for diagnosing dermatological conditions, while "black light posters" are more entertaining. In addition, some fluorescent materials emit light in the infrared.

Within the graphics community, Glassner [7] followed by Wilkie et al. [18] rendered fluorescent objects as diffuse, and Hullin et al. [19] claim that they are "weakly directional". These works explain this observation by the fact that the fluorescence emission does not originate from the surface, but from subsurface processes. In addition, it is important to realize that even before the subsurface scattering takes place, the angular distribution of fluorescence from particles itself was measured to be isotropic in most cases [20,21]. This isotropic emission from the particles manifests as isotropic emission from the surface if the fluorescent particles are uniformly spread in the object and are relatively close to the surface. The reflectance and scattering processes are demonstrated in Fig. 3. Incident light may specularly reflect off of the surface and the observed color is often that of the illuminant (a). Diffuse reflectance may not be ideally Lam-

¹ For better color quality, please view all the images in the paper on a computer screen.

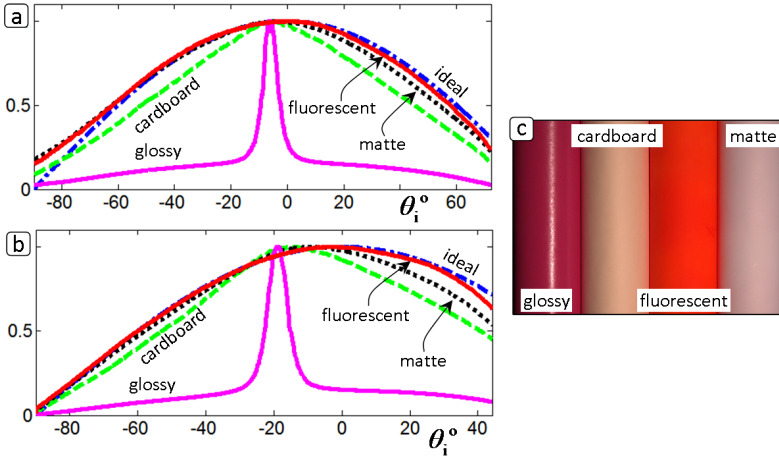


Fig. 4. Examination of the angular dependency of the fluorescent emission: (a,b) The normalized intensity of several spray-painted paper sheets wrapped around a cylinder is plotted as a function of incident angle θ_i , for two light source positions. The incident angle was estimated using a spherical light probe. The specular reflection from the glossy paint indicates the location of the specular peak. The non-ideal diffuse peaks are shifted from the ideal Lambertian peak towards the specular direction. From all the measured surfaces, the fluorescent surface is the closest to the ideal reflection. Interestingly, the reflection from the cardboard is significantly less diffuse than that of the matte paint; (c) Images of the four materials. The cylinders are adjacent for display purposes, but the measurements were done separately to avoid inter-reflections.

bertian (b), and the fluorescence emission (c) is observed to be closer to ideal Lambertian. For subsurface particles, differences in optical path length from the fluorescence emission to the surface may manifest as a non-isotropic fluorescence emission, due to absorption [22] of the object material (d), especially in wider viewing angles. This means that not all fluorescence emissions are ideally Lambertian throughout the entire viewing range. Characterizing the nature of these cases requires future work. Here, following the above analysis, in the next section we provide an empirical demonstration of fluorescent emission that follows Lambert's law, and in the rest of the paper we demonstrate how to use this insight for shape estimation.

3 Angular Dependency of Fluorescent Emission

In this section we verify the claim that the fluorescence emission is well approximated by an ideal Lambertian model through a simple experiment. We image a cylinder, illuminated with a distant collimated light source, such that the light source direction and strength is uniform across the cylinder. The cylinder provides imaging of all incident directions in a single image. The light source direction is determined using a light probe (mirrored sphere) in the scene.

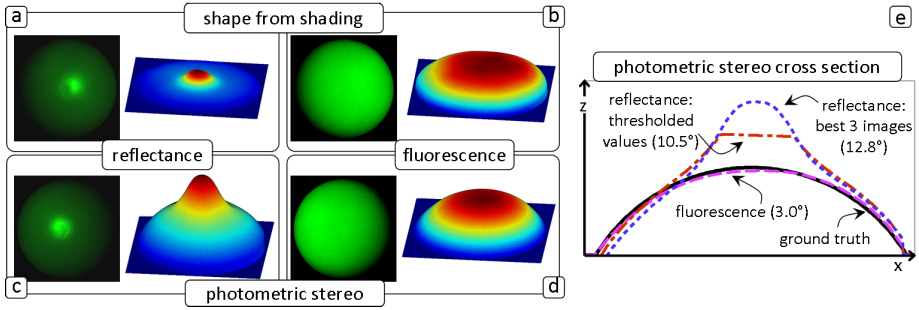


Fig. 5. Shape reconstructions of a sphere spray painted with green fluorescent paint, using reflectance and fluorescence channels. In both setups, the green channel is used. (a,b) Reconstruction using shape from shading. The reconstruction from reflectance has a clear bump from specularities. In the reconstruction from fluorescence, the reconstruction is not ideal but closely resembles the shape of a sphere. (c,d) Reconstruction by photometric stereo. In the reconstruction from reflectance, for each pixel, we use the 3 frames that are the least bright in this pixel, to reduce the effect of the specular reflection. Still, the reconstruction from fluorescence is almost ideal, whereas the reconstruction from reflectance suffers from its non-Lambertian nature. Note that both images in (b,d) appear very diffuse. (e) Cross sections of the different reconstructions. Values in parenthesis depict the mean error in degrees of the normal angles in each reconstruction.

To compare reflectance properties, we spray-painted paper sheets with several types of paint: matte, glossy, and fluorescent. These were imaged under a few light source directions. Fig. 4 depicts the intensity plots as a function of θ_i for two distinct light source positions in addition to the expected ideal Lambertian. The normal direction at each pixel is obtained from its position on the cylinder and the known radius of the cylinder. Measurements along lines with constant surface were averaged to remove noise, and the brightness was normalized to have a consistent maximum intensity. At all measured light source directions, the fluorescent surface is closer to the ideal reflection than the other surfaces.

In all experiments reported in this paper we use raw images acquired either with a Canon 1D mark IV or with a Canon 5DII illuminated with a Lowel pro-light tungsten halogen light source. The reflectance images were imaged with this setup as-is and all the fluorescence images were imaged using a blue filter on the light source and a yellow filter mounted on the lens acquired from NightSea LLC. For Chlorophyll fluorescence images, we use a Canon 5DII with a removed IR filter, for increased sensitivity for Chlorophyll fluorescence [15].

4 Shape from Shading

Eq. (4) is used in various methods for reconstructing 3D shape as it provides a simple relation between image intensity and object normals, provided the surface is indeed ideally Lambertian and the light source is distant. In shape from shading methods, a single image is used to estimate the shape under the assumption

of constant albedo [23]. A unit normal at each pixel is defined by two unknowns, and Eq. (4) provides a single constraint. Then, various additional constraints, such as integrability and smoothness are applied to obtain a solution. There is also a bulk of literature on numerical methods for integrating the normals into a smooth surface [23,24]. The majority of the existing methods assume Lambertian reflectance and even then it is commonly acknowledged that results are usually unsatisfactory. A few methods consider non-Lambertian reflectance models, that are known a-priori, e.g. [25].

Here we show that the Lambertian-like fluorescence emission is an ideal input to shape from shading. We imaged a sphere spray-painted with green fluorescent paint. In each case (reflectance and fluorescence) the green image channel is the input to shape from shading. The reconstruction was performed using code based on [26], and the recovered shapes are shown in Fig. 5. The reflectance suffers from the specular reflection, whereas in the reconstruction from fluorescence, the reconstruction is not ideal but very closely resembles the shape of a sphere.

5 Calibrated Photometric Stereo

As stated in the previous section, shape from a single image usually produces unsatisfiable results due to its under-determined nature and the required constant albedo assumption. Therefore, in photometric stereo methods at least three images are taken [2], in order to have a fully determined set of equations from the form of Eq. (4). The problem can be cast as a matrix equation, where for each pixel

$$\mathbf{I}_{k \times 1} = \mathbf{S}_{k \times 3} \mathbf{N}_{3 \times 1} . \quad (6)$$

Here \mathbf{S} is a $k \times 3$ matrix, representing k distinct light source directions normalized by their intensity. The pixel values under each light source are stacked in $\mathbf{I}_{k \times 1}$. In the calibrated case, the light source directions \mathbf{S} are known and thus \mathbf{N} can be solved for directly from Eq. (6) given at least three linearly independent light source locations.

The majority of photometric stereo methods assumes Lambertian surfaces, while some works assume a different known reflectance function, explicit or parametric, e.g. [27]. There are also attempts to estimate spatially varying BRDFs [28]. Considerable effort is given to remove specularities in the images, usually assuming dichromatic BRDFs [29,30].

Here, we show how the fluorescence signal provides an ideal input to Eq. (6) and alleviates the need for more complex methods. In Fig. 5 we show the result of photometric stereo on a sphere spray painted with green fluorescent spray. In the reconstruction from reflectance, we tried two methods to reduce the effect of the non-Lambertian reflectance. In one, for each object point we used only the three frames where the corresponding pixel was the least bright. In the second, we manually thresholded the brightest areas, and only use the non-thresholded frames for each object point. A normal pointing in the z direction was assigned to object points that did not have at least three input frames after thresholding. Still, the reconstruction from fluorescence is much closer to the ground truth.

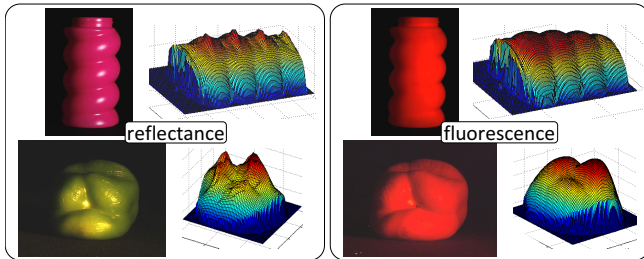


Fig. 6. 3D reconstruction using photometric stereo applied to a fluorescent pink plastic bottle (top) and to a (real) green bell pepper (bottom). These objects fluoresce as-is and were not painted. [Left] The reflectance images have clear specularities that harm the reconstruction. [Right] The fluorescence images are very diffuse and thus the reconstruction based on them does not suffer from these problems. For all objects the fluorescence image was taken from the red camera channel, and the reflectance image was from the blue channel. Seven images were used to reconstruct the bottle while nine were used for the pepper.

The cross sections of the different reconstructions and the mean error of the reconstructed normal angles are depicted in Fig 5(e).

Reconstruction of more complex objects is shown in Fig. 6. We show reconstruction for a fluorescent plastic bottle (top) and for a (real) green bell pepper (bottom). In addition, Fig. 7 shows another reconstruction of a fluorescent toy squirt gun. All objects fluoresce as-is and were not painted (see Sec. 3). In all cases the reflectance image (left) has clear specularities that harm the reconstruction. The fluorescence images (right) appear very diffuse and indeed the reconstruction based on them does not suffer from problems common to non-ideal diffuse surfaces. For all objects the fluorescence image is taken from the red camera channel, and the reflectance is from the blue channel. The integration part in the reconstruction uses the method in [31].

6 Uncalibrated Photometric Stereo

The input to uncalibrated photometric stereo is a set of images of an object in fixed pose under unknown lighting conditions. i.e., no information about the light source strength or direction is needed [32,33]. The basic equation describing the problem is then

$$\mathbf{I}_{k \times j} = \mathbf{S}_{k \times 3} \mathbf{N}_{3 \times j} \quad , \quad (7)$$

where j is the number of pixels in the image. The unknown light source directions \mathbf{S} are considered uniform for all j pixels in the image. Image intensity of all pixels under all light sources $\mathbf{I}_{k \times j}$ is used as an input, to simultaneously estimate \mathbf{S} and the normal directions at every pixel, $\mathbf{N}_{3 \times j}$. When the object is Lambertian and assuming only local reflectance, Eq. (7) can be solved using SVD and applying integrability constraints up to a generalized bas relief (GBR) transformation [33,34] in the form

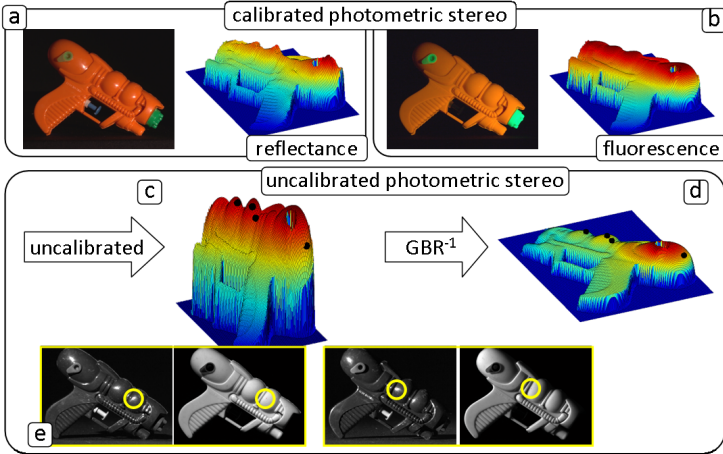


Fig. 7. (a,b) Calibrated photometric stereo from fluorescence, demonstrated on a fluorescent orange toy squirt gun, using 12 images. The fluorescence signal is diffuse, providing a 3D reconstruction that does not suffer from bumps due to specularities. (c-e) Here we show how specular pixels from the *reflectance* image (originally not used for reconstruction) can be used to resolve GBR ambiguity in uncalibrated photometric stereo from the *fluorescence* channel. (c) The solution for the uncalibrated case, based on [33], using the input images used in (b). The shape of the squirt gun is apparent, but skewed with a GBR. Then, specular pixels are chosen (marked by black spheres). These pixels imply constraints that allow recovery of the correct GBR transformation, following Eq. (9). The successfully transformed reconstruction is shown in (d). In (e) two examples of the actual input images (both reflectance and fluorescence) are shown and the specular location is marked. Note that the reflection channel is used solely for locating the specularity while surface is densely reconstructed from the more stable fluorescence channel which does not exhibit specularities at these (or any) pixels.

$$G = \begin{pmatrix} 1 & 0 & 0 \\ 0 & 1 & 0 \\ \mu & \nu & \tau \end{pmatrix}, \quad (8)$$

where μ , ν and τ are the three degrees of freedom of the transformation.

For strictly Lambertian surfaces, inter-reflections in concave regions can resolve the GBR [35] as can heuristics like minimization of the entropy of albedo [36]. However, both constraints are not always effective. Alternatively, the GBR can be resolved using isotropy together with Helmholtz reciprocity [37]. This method can only be accomplished when the Lambertian component of reflectance can be separated from the specular component (e.g., using polarization [38] or the SUV color space under the dichromatic reflectance model [39]).

Here, we offer a method to resolve the GBR in color images when the fluorescence is in one color channel and other color channels contain reflectance images of a specular surface. The strategy is simple. Because the emitted radiance due to fluorescence behaves like a Lambertian surface, the surface can be reconstructed

up to a GBR transformation from the fluorescence channel of multiple images under unknown lighting using the method of Yuille and Snow [33]. The GBR can then be resolved from the specularities detected in the reflectance channel using the method of Drbohlav and Chaniler [40]. This method uses normals from at least two specular points to impose constraints on the reconstruction of the form

$$\mathbf{v} = 2(\mathbf{n} \cdot \mathbf{l})\mathbf{n} - \mathbf{l} , \quad (9)$$

where \mathbf{v} is the viewing direction, \mathbf{n} is the unknown normal at the specular point and \mathbf{l} is the unknown light source direction at the specific image containing the specular point. The constraint in Eq. (9) is imposed on the solution of the uncalibrated step [33] to estimate the correct GBR transformation.

In [40], the normals reconstructed from the specular pixels in the reflectance image are actually used in Eq. (9) to impose the constraint for surface reconstruction. Thus, they are prone to errors and to an unstable reconstruction. As opposed to that, in our case we have a clear advantage as the normals in the uncalibrated solution are obtained from the Lambertian *fluorescence* channel, and the *reflectance* channel is used solely to locate the specular pixels. We show an example for this method in Fig. 7(c-e). The uncalibrated case is solved up to a GBR ambiguity, and then the transformation is estimated based on specularities. In our experience, this method sometimes actually produces results that are better than the calibrated results due to better accuracies in estimating the light source directions.

7 Mutual Illumination in Reconstruction

Nearly all radiometric methods for shape reconstruction (shape-from-shading, photometric stereo) are based on local illumination models wherein the image irradiance is a function of the direct illumination from the light source onto an imaged surface patch and the patch properties. Unless methods to separate local and global illumination [41] are applied, the inter-reflections of light from other surfaces in the scene onto the patch are neglected and left unmodeled. However, when rendering scenes in computer graphics, global illumination methods achieve their realism precisely because they account for inter-reflections. Forsyth and Zisserman showed that the image intensity of a dihedral (where two planar faces meet and form a concavity) becomes brighter closer to the corner due to mutual illumination, and the increase of brightness is related to the albedos of the two faces [42]. When performing reconstruction using shape-from-shading or photometric stereo, this increased brightness results in shallower reconstructed concavities than the true depth. Nayar et. al. [43] called this the pseudo surface, and introduced an iterative method for estimating the true surface from the pseudo surface by estimating an inter-reflection kernel at each step.

Consider a simple concavity illuminated solely by wavelengths within its fluorescence excitation spectrum. Some of the incident light will reflect from the surface according to its BRDF, and some amount will excite fluorescence that will be emitted according to the material's emission spectrum. In general, the

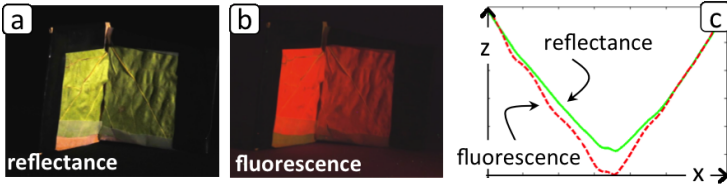


Fig. 8. To demonstrate how fluorescence helps avoid mutual illumination, we covered a V-shaped cardboard with leaves. (a,b) The reflectance and the fluorescence images of the covered cardboard; (c) The shape was reconstructed using calibrated photometric stereo for both the reflectance and fluorescence channels. The reconstructed depth (at a certain cross section) is plotted for the reflectance and fluorescence images. While the reconstruction from the reflectance channel shows classical bending of the corner (pseudo surface) as described in [43], the reconstruction from the fluorescence channel maintains sharp edges clearly demonstrating the reduction of the effect of inter-reflections.

reflected light from the fluorescence emission can interreflect within the concavity. However, when the material *does not* reflect light at the wavelengths of the fluorescence emission, there will not be any subsequent interreflections of the fluorescence emissions. Consequently, reconstruction methods that only assume local Lambertian reflectance will be effective for images of such materials.

Contrary to [8], we found that most artificial fluorescent objects and materials reflect the color they fluoresce, as they are made fluorescent to appear brighter than they are, in the same color. However, many natural objects such as leaves, vegetables and fruits, fluoresce at different wavelengths than they reflect. For example, green leaves reflect green light but absorb red and blue light. When lit by blue light, the Chlorophyll in the leaves will fluoresce red (Fig. 1). Because the leaf absorbs red light, we do not expect appreciable brightening due to inter-reflections. Consequently, when performing reconstruction, local illumination models will be adequate to correctly estimate the depth, and methods such as [41,43] should be unnecessary.

To demonstrate this claim on a simple case, we created a concave dihedral (V-shaped) out of cardboard and glued leaves to it, such that it is covered by the leaves. Using the reflectance and fluorescence channels separately, the shape was reconstructed using calibrated photometric stereo (example images shown in Fig. 8a,b, total images was 10). To clearly demonstrate the effect, we plot a cross section of the reconstructed height for the two channels, (Fig. 8c). Whereas the reconstruction from the fluorescence channel shows a sharp corner, the reconstruction from the reflectance channel is shallower and the smooth rounding of the corner (pseudo surface) is similar to what is described in [43].

8 Summary

Imaging fluorescence through inexpensive off-the-shelf filters opens an enchanting world of glowing objects and objects that alter their color appearance. It

is surprising to discover that many every day objects fluoresce in the visible spectrum under UV or blue light and therefore can be imaged with conventional cameras. In this paper we showed the benefit of using fluorescence for 3D reconstruction methods since fluorescence emissions are often isotropic much like ideal Lambertian reflectance. This insight can be used, for example, for 3D reconstruction of fluorescent corals underwater, where texture correspondences are sometimes problematic, given the water optical properties are taken into account. We showed that there is an advantage of imaging a fluorescent object over a matte object, as specularities from the reflectance channel can provide additional information regarding light source directions relative to the object. In addition, we showed how in some cases fluorescence can avoid mutual illumination problems.

In some cases, the fluorescence emission might not be ideally Lambertian due to differences in subsurface absorption. The characterization of such cases requires more measurements of different fluorescent materials. When the emitted radiance due to fluorescence is isotropic, other computer vision methods that rely on the constant brightness assumption such as binocular stereopsis, multi view reconstruction, and optical flow estimation can be applied to fluorescence images. However, fluorescence typically does not exhibit the same type of spatial/texture variation as would be found with reflectance texture, and this might provide an alternate set of challenges.

Acknowledgments. The work was supported by NSF grant ATM-0941760. Tali Treibitz is an Awardee of the Weizmann Institute of Science – National Postdoctoral Award Program for Advancing Women in Science.

References

1. Barnard, K.: Color constancy with fluorescent surfaces. In: Proc. IS&T/SID Seventh Color Imaging Conference: Color Science, Systems and Applications (1999)
2. Woodham, R.: Photometric method for determining surface orientation from multiple images. *Opt. Eng.* 19, 139–144 (1980)
3. Silver, W.M.: Determining shape and reflectance using multiple images. Master's thesis, Massachusetts Institute of Technology (1980)
4. Guilbault, G.: Practical fluorescence, vol. 3. CRC (1990)
5. Ihrke, I., Goidluecke, B., Magnor, M.: Reconstructing the geometry of flowing water. In: Proc. IEEE ICCV (2005)
6. Hullin, M., Fuchs, M., Ihrke, I., Seidel, H., Lensch, H.: Fluorescent immersion range scanning. *ACM TOG* 27 (2008)
7. Glassner, A.: Principles of Digital Image Synthesis, ch. 17. Morgan Kaufmann Publishers (1995)
8. Sato, I., Okabe, T., Sato, Y.: Bispectral photometric stereo based on fluorescence. *Trans. IEEE CVPR* (2012)
9. Szeliski, R.: Computer vision: Algorithms and applications. Springer (2010)
10. Horn, B.: Robot vision, ch. 10. The MIT Press (1986)
11. Oren, M., Nayar, S.: Generalization of the lambertian model and implications for machine vision. *IJCV* 14, 227–251 (1995)

12. Phong, B.: Illumination for computer generated pictures. *Communications of the ACM* 18, 311–317 (1975)
13. Cook, R., Torrance, K.: A reflectance model for computer graphics. *ACM TOG* 1, 7–24 (1982)
14. Ashikhmin, M., Shirley, P.: An anisotropic phong BRDF model. *J. of Graphics Tools* 5, 25–32 (2000)
15. Treibitz, T., Neal, B.P., Roberts, P., Kline, D.I., Beijbom, O., Belongie, S., Mitchell, B.G., Jaffe, J., Kriegman, D.: Wide field of view full spectrum fluorescence imaging for coral ecology. In: *International Coral Reef Symposium* (2012)
16. Zhang, C., Sato, I.: Separating reflective and fluorescent components of an image. In: *Proc. IEEE CVPR* (2011)
17. Alterman, M., Schechner, Y., Weiss, A.: Multiplexed fluorescence unmixing. In: *Proc. IEEE ICCP* (2010)
18. Wilkie, A., Weidlich, A., Larboulette, C., Purgathofer, W.: A reflectance model for diffuse fluorescent surfaces. In: *Proc. Int. Conf. Comp. graphics & interactive techniques in Australasia and Southeast Asia*, pp. 321–331 (2006)
19. Hullin, M., Hanika, J., Ajdin, B., Seidel, H., Kautz, J., Lensch, H.: Acquisition and analysis of bispectral bidirectional reflectance and reradiation distribution functions. *ACM TOG* 29 (2010)
20. Kratochvil, J., Lee, M., Kerker, M.: Angular distribution of fluorescence from small particles. *Applied Optics* 17 (1978)
21. Gordon, H., Voss, K., Kilpatrick, K.: Angular distribution of fluorescence from phytoplankton. *Limnology and Oceanography*, 1582–1586 (1993)
22. Collins, D., Kiefer, D., Soohoo, J., Stuart McDerimid, I.: The role of reabsorption in the spectral distribution of phytoplankton fluorescence emission. *Deep Sea Research Part A. Oceanographic Research Papers* 32, 983–1003 (1985)
23. Zhang, R., Tsai, P., Cryer, J., Shah, M.: Shape-from-shading: a survey. *IEEE Trans. PAMI* 21, 690–706 (1999)
24. Durou, J., Falcone, M., Sagona, M.: Numerical methods for shape-from-shading: A new survey with benchmarks. *Computer Vision and Image Understanding* 109, 22–43 (2008)
25. Ahmed, A., Farag, A.: A new formulation for shape from shading for non-lambertian surfaces. In: *Proc. IEEE CVPR* (2006)
26. Tsai, P.S., Shah, M.: Shape from shading using linear approximation. *Image and Vision Computing* 12, 487–498 (1994)
27. Tagare, H., Defigueiredo, R.: A theory of photometric stereo for a class of diffuse non-lambertian surfaces. *IEEE Trans. PAMI* 13, 133–152 (1991)
28. Goldman, D., Curless, B., Hertzmann, A., Seitz, S.: Shape and spatially-varying BRDFs from photometric stereo. *IEEE Trans. PAMI* 32, 1060–1071 (2010)
29. Sato, Y., Ikeuchi, K.: Temporal-color space analysis of reflection. *JOSA A* 11, 2990–3002 (1994)
30. Zickler, T., Mallick, S., Kriegman, D., Belhumeur, P.: Color subspaces as photometric invariants. *IJCV* 79, 13–30 (2008)
31. Frankot, R., Chellappa, R.: A method for enforcing integrability in shape from shading algorithms. *IEEE Trans. PAMI* 10, 439–451 (1988)
32. Hayakawa, H.: Photometric stereo under a light-source with arbitrary motion. *JOSA-A* 11, 3079–3089 (1994)
33. Yuille, A., Snow, D.: Shape and albedo from multiple images using integrability. In: *Proc. IEEE CVPR* (1997)
34. Belhumeur, P., Kriegman, D., Yuille, A.: The bas-relief ambiguity. *IJCV* 35 (1999)

35. Chandraker, M., Kahl, F., Kriegman, D.: Reflections on the generalized bas-relief ambiguity. In: Proc. IEEE CVPR (2005)
36. Alldrin, N.G., Mallick, S., Kriegman, D.: Resolving the generalized bas-relief ambiguity by entropy minimization. In: Proc. IEEE CVPR (2007)
37. Tan, P., Mallick, S., Quan, L., Kriegman, D., Zickler, T.: Isotropy, reciprocity and the generalized bas-relief ambiguity. In: Proc. IEEE CVPR (2007)
38. Nayar, S., Fang, X., Boulton, T.: Separation of reflection components using color and polarization. *IJCV* 21, 163–186 (1997)
39. Zickler, T., Mallick, S., Kriegman, D., Belhumeur, P.N.: Color subspaces as photometric invariants. *IJCV* 79, 13–30 (2008)
40. Drbohlav, O., Chanlier, M.: Can two specular pixels calibrate photometric stereo? In: Proc. IEEE ICCV (2005)
41. Nayar, S., Krishnan, G., Grossberg, M., Raskar, R.: Fast separation of direct and global components of a scene using high frequency illumination. *ACM TOG* 25, 935–944 (2006)
42. Forsyth, D., Zisserman, A.: Mutual illumination. In: Proc. IEEE CVPR (1989)
43. Nayar, S., Ikeuchi, K., Kanade, T.: Shape from interreflections. In: Proc. IEEE ICCV (1990)